Atmos. Meas. Tech. Discuss., 8, 8439–8481, 2015
www.atmos-meas-tech-discuss.net/8/8439/2015/
doi:10.5194/amtd-8-8439-2015

Atmospheric Measurement Techniques Discussions

Sensitivity of thermal infrared sounders to the chemical and micro-physical properties of UTLS secondary sulphate aerosols

P. Sellitto and B. Legras

Laboratoire de Météorologie Dynamique (LMD), CNRS-UMR8539, Institut Pierre Simon Laplace, École Normale Supérieure, École Polytechnique, Université Pierre et Marie Curie, Paris, France

Received: 28 June 2015 – Accepted: 24 July 2015 – Published: 10 August 2015

Correspondence to: P. Sellitto (psellitto@lmd.ens.fr)

Published by Copernicus Publications on behalf of the European Geosciences Union.

Abstract

Monitoring upper tropospheric-lower stratospheric (UTLS) secondary sulphate aerosols and their chemical and micro-physical properties from satellite nadir observations is crucial to better understand their formation and evolution processes and then to estimate their impact to the UTLS chemistry, and on regional and global radiative balance. Here we present a study aimed at the evaluation of the sensitivity of thermal infrared (TIR) satellite nadir observations to the chemical composition and the size distribution of idealized UTLS sulphate aerosol layers. The extinction properties of sulphuric acid/water droplets, for different sulphuric acid mixing ratios and temperatures, are systematically analysed. The extinction coefficients are derived by means of a Mie code, using refractive indexes taken from the GEISA (Gestion et Étude des Informations Spectroscopiques Atmosphériques: Management and Study of Spectroscopic Information) spectroscopic database and log-normal size distributions with different effective radii and number concentrations. IASI (Infrared Atmospheric Sounding Interferometer) pseudo-observations are generated using forward radiative transfer calculations performed with the 4A (Automatized Atmospheric Absorption Atlas) radiative transfer model, to estimate the impact of the extinction of idealized aerosol layers, at typical UTLS conditions, on the brightness temperature spectra observed by this satellite instrument. We found a marked and typical spectral signature of these aerosol layers between 700 and 1200 cm^{-1}, due to the absorption bands of the sulphate and bi-sulphate ions and the undissociated sulphuric acid, with the main absorption peaks at 1170 and 905 cm^{-1}. The dependence of the aerosol spectral signature to the sulphuric acid mixing ratio, and effective number concentration and radius, as well as the role of interferring parameters like the ozone, sulphur dioxide, carbon dioxide and ash absorption, and temperature and water vapour profile uncertainties, are analyzed and critically discussed.

AMTD
8, 8439–8481, 2015

1 Introduction

Secondary sulphate aerosols are sulphate-containing aqueous solution droplets, generally of sub-micron size, produced from gas-to-particle conversion processes involving sulphur-containing gaseous precursors (Hamill et al., 1997). They are one of the predominant typologies of aerosols in the upper troposphere/lower stratosphere (UTLS) (SPARC, 2006; Sheng et al., 2015; Yu et al., 2015) and can have an important impact on the atmospheric radiative transfer and climate (see, e.g., Robock and Oppenheimer, 2003), cirrus formation and their optical properties (see, e.g., Gettelman et al., 2012), and chemistry in the UTLS (see, e.g., von Glasow et al., 2009). Monitoring their chemical composition, i.e., the mixing ratio of sulphates in the aqueous solution, and their micro-physical properties, i.e., the size distribution parameters, is fundamental to better understand the processes of formation and their impacts on UTLS chemistry and radiative transfer. From a satellite perspective, limb-viewing and occultation UV/VIS/NIR and TIR instruments, e.g., the Stratospheric Aerosol and Gas Experiment (SAGE) II and III (e.g., Thomason et al., 1997; Bauman et al., 2003), the Improved Stratospheric and Mesospheric Sounder (ISAMS) (e.g., Grainger et al., 1993; Echle et al., 1998), the Atmospheric Trace Molecule Spectroscopy (ATMOS) (e.g., Eldering et al., 2004), the Optical Spectrograph and Infrared Imager System (OSIRIS) (e.g., Bourassa et al., 2010) and Atmospheric Chemistry Experiment (ACE) (e.g., Doeringer et al., 2012) have been used to derive vertical profiles of UTLS sulphate aerosol absorption, especially during strong volcanic eruptions. Even if these observations have allowed the identification of the perturbation of the UTLS aerosol layer produced by stronger volcanic eruptions, a quantitative characterization of the aerosol by means of the chemical and micro-physical parameters of the layer has not been systematically attempted. In addition, limb and occultation observations are not well adapted to monitor the processes of formation and evolution of the aerosol population due to the low horizontal resolution and the scarce distribution of observations. Routine nadir measurements are more adapted to monitor sulphate aerosols properties from the regional to global scale, to

AMTD
8, 8439–8481, 2015

constrain processes and to estimate the global impact of sulphate aerosols production and evolution, due to the their extended spatial coverage and higher spatial resolution. Nadir satellite observations in the solar spectral range (ultraviolet, visible, near infrared: UV/VIS/NIR) are insensitive to the chemical composition of aerosols, while they can provide a partial information on their size distribution, via the fine-to-coarse aerosol optical depth ratio (Kaufman et al., 2005; Remer et al., 2005). Thermal InfraRed (TIR) observations are sensitive to the chemical composition of the aerosols due to the strong spectral variations of the imaginary part of the refractive index in this band, and then of the absorption, as a function of the composition (e.g., Clarisse et al., 2013). Unfortunately, the exploitation of nadir TIR observations for the sulphate aerosol layer monitoring consists, today, only in a semi-quantitative detection (Clarisse et al., 2013), as nadir observations are generally regarded as weakly sensitive to the relatively small and diluted (in terms of their number concentration) sulphate aerosol droplets. As a consequence, despite their importance, the satellite observation at the regional scale of sulphate aerosols in the UTLS and their properties is limited.

In this work, we present an analysis of the sensitivity of the satellite nadir TIR observations to secondary sulphate aerosols in the UTLS and their chemical and microphysical properties. The main target of this paper is to link the optical characterization of sulphate solutions, as available from the published spectroscopic laboratory measurements of, e.g., Biermann et al. (2000), to the empiric observation of aerosols signatures in favourable natural contexts, e.g., for volcanically enhanced sulphates production in the UTLS. Indeed, a peculiar aerosol signature (increasing absorption between about 700 and 1300 cm^{-1}) has been observed in the past in those conditions, e.g., by Clarisse et al. (2013) for the eruption of the Sarychev volcano or by Grainger et al. (1993) for the eruption of the Pinatubo volcano. These signatures have been attributed to the secondary sulphate aerosols formed in the volcanic plume, without linking them to the specific spectroscopic features of the different sulphates contained in the droplets and their chemical and micro-physical characterization. Establishing such a link will improve our understanding of the radiative properties of these aerosol layers and is a prerequi-

AMTD
8, 8439–8481, 2015

site for an optimal retrieval of their properties from satellite data. To do so, the extinction properties of sulphuric acid/water droplets, for different sulphuric acid mixing ratios and temperatures, are systematically analysed. The extinction coefficients are derived by means of a Mie code, using refractive indices taken from the GEISA (Gestion et Étude des Informations Spectroscopiques Atmosphériques: Management and Study of Spectroscopic Information) spectroscopic database and log-normal size distributions with different effective radii and number concentrations. IASI (Infrared Atmospheric Sounding Interferometer) pseudo-observations are generated using forward radiative transfer calculations performed with the 4A (Automatized Atmospheric Absorption Atlas) radiative transfer model, to estimate the impact of the absorption of idealized aerosol layers, at typical UTLS conditions, on the brightness temperature (BT) spectra observed by this simulated satellite instruments.

The paper is organized as follows. In Sect. 2 we introduce the data and methods used in our study. In Sect. 3 we discuss the spectral absorption of the sulphate aerosol layer, and the dependence from its chemical and micro-physical properties. The IASI pseudo-observations obtained using these aerosol optical characterizations are discussed in Sect. 4, and the UTLS sulphate aerosol BT signature is isolated and analyzed with respect to the chemical and micro-physical properties of the layer. The role of interferring parameters, e.g., the uncertainties of the temperature, and water vapour and ozone concentration profiles, as well as the absorption by other volcanic species as SO_2, CO_2 and ash, are discussed in Sect. 5. Conclusions are drawn in Sect. 6.

2 Data and methods

To analyze the sensitivity of nadir satellite observations in the TIR spectral region, we have generated a set of IASI pseudo-observations with the Automatized Atmospheric Absorption Atlas OPerational (4A/OP) radiative transfer model, (see, e.g., Scott and Chedin, 1981). 4A/OP is a fast and accurate line-by-line radiative transfer model, developed by the Laboratoire de Météorologie Dynamique and the NOVELTIS company

AMTD
8, 8439–8481, 2015

(http://www.noveltis.com/), with the support of the CNES (Centre National d'Études Spatiales), to simulate the radiative transfer in planetary atmospheres, with a particular target on the IR spectral region. In Tjemkes et al. (2003) 4A/OP simulations, as well as simulations from other 9 radiative transfer models, were compared to IR high spectral resolution observations and found capable of reproducing the observations to within the observation noise. 4A/OP has been used in support of the IASI missions (Jacquinet-Husson et al., 2003). Please refer to the website http://4aop.noveltis.com/ for more details on 4A/OP.

In the present work, IASI observations are simulated by means of the observation geometry, the instrument spectral response function (ISRF) and the radiometric noise. Typical nadir observations have been considered, with zero viewing zenith angle. We have simulated radiances in the range 700.0–1300.0 cm^{-1}, with a spectral resolution of 0.25 cm^{-1} before apodization (0.50 cm^{-1} apodized spectral resolution), a spectral sampling of 0.25 cm^{-1} and a Gaussian ISRF. The radiometric noise is set at a noise equivalent brightness temperature of 0.25 K. These parameters are implemented into the standard distribution of 4A/OP, and based on IASI preparatory studies (see, e.g., Tournier et al., 2002).

A baseline 4A/OP run, i.e., a run with no sulphate aerosols, is first performed to compare with different configurations of the UTLS sulphate aerosols layer, i.e., with different chemical and micro-physical properties. Then different runs with varying H_2SO_4 mixing ratios and aerosol size distributions are performed. For all these simulations, a typical tropical atmosphere, in terms of temperature, pressure and trace gases vertical profiles, is considered. The altitude of the sulphate aerosol layer has been fixed at about 150 hPa. 4A/OP is capable to simulate aerosols scattering and absorption by means of the DISORT (Discrete Ordinate Radiative Transfer) scheme, using the extinction (absorption plus scattering) coefficient, the single scattering albedo and the asymmetry parameter as optical inputs. These optical parameters for the different simulated sulphate aerosols layers are obtained with the IDL (Interactive Data Language, http://www.exelisvis.com/ProductsServices/IDL.aspx) Mie scattering routines of

AMTD
8, 8439–8481, 2015

the Earth Observation Data Group of the Department of Physics of Oxford University. Starting from the refractive index and the size distribution of the aerosol layer, the Mie theory allows the calculation of the extinction, scattering and absorption coefficients, as well as derived quantities like the single scattering albedo, and the angular distribution of the radiation fields (by means of the phase function), which can be represented by the integral asymmetry parameter (van de Hulst, 1957).

In this work we assume that that sulphate aerosols are binary systems of H_2SO_4/H_2O solution droplets, with varying H_2SO_4 mixing ratios. Ternary $HNO_3/H_2SO_4/H_2O$ solutions, which are important for nitric acid hydrates formation in polar stratospheric clouds (Knopf et al., 2002), are excluded from this study. We have used temperature dependent refractive indices for different mixing ratios of the binary system H_2SO_4/H_2O from the laboratory study of Biermann et al. (2000). These data are available from the GEISA database (Jacquinet-Husson et al., 2008). Refractive indices are available for a wide array of temperatures, from 183 to 293 K, and H_2SO_4 mixing ratios (in mass, i.e. the ratio of the H_2SO_4 mass to the total mass of the droplets) ranging from 10 to 80 %, so covering tropospheric and stratospheric conditions. These refractive indices are measured in the region 500.0–5000.0 cm^{-1}, where major features of the absorption spectra of sulphate droplets-radiation can be found, i.e., the OH stretching region (3200–3500 cm^{-1}), bi-sulphate ion absorption (1341, 1030, 1050, 885 and 593 cm^{-1}) and sulphate ion absorption (1104 and 613 cm^{-1}). For higher concentrations, features of the undissolved H_2SO_4 molecules (absorption at 1370, 1170, 965, 905 and 564 cm^{-1}) appear as well. Please refer to (Biermann et al., 2000) for more details on this dataset and to, e.g., Miller et al. (2005) and Boer et al. (2007) for a detailed description of the spectroscopic absorption vibration modes for the sulphate and bi-sulphate ions, and the sulphuric acid molecule.

The size distributions for our simulated layers (i.e., a function $n(r)$ defined so that $n(r)\mathrm{d}r$ is the number of particles per unit volume, with radius between r and $r+\mathrm{d}r$) are

AMTD
8, 8439–8481, 2015

modelled as log-normal distributions:

$$n(r) = \frac{N_0}{r \ln \sigma_r \sqrt{2\pi}} e^{-\frac{1}{2}\left(\frac{\ln(r/r_m)}{\ln \sigma_r}\right)^2} \quad (1)$$

In Eq. (1), N_0 is the total number concentration (in particles cm^{-3}), r_m is the mean radius and $\ln \sigma_r$ is the unitless standard deviation of $\ln(r/r_m)$. For our simulations, we fixed σ_r to 1.86 (a typical value, see, e.g. SPARC, 2006) and we varied N_0 and r_m, to study the impact of different number concentrations and mean size on the absorption properties of the sulphate aerosol layers. We simulate layer with N_0 = 8, 9, 10, 12, 15, 20, 25 and 30 particles cm^{-3}, and r_m = 0.06, 0.07, 0.08, 0.1, 0.15, 0.2, 0.3 and 0.4 µm. Here we recall that a typical UTLS sulphate aerosol layer in background conditions, i.e., without any perturbation from sulphur compounds emissions from natural (volcanic explosive eruptions) or anthropic (severe UTLS pollution) sources, can be represented by a log-normal distribution with N_0 of a few particles cm^{-3} and a r_m lower than 0.1 µm, while a volcanically perturbed layer can be represented by a log-normal distribution with N_0 of a few tents particles cm^{-3} and a r_m higher than 0.2 µm (SPARC, 2006). Thus, our database can represent several naturally occurring conditions. It must be noted here that multi-modal log-normal distributions have also been observed, especially in volcanically perturbed situations (see, e.g., Deshler et al., 2003), but are not simulated in the present study. We plan in the future to extend our simulations to multi-modal log-normal size distributions.

From H_2SO_4 concentration and aerosol size distribution, other parameters can be derived, which are useful metrics for remote sensing measurements. It is often convenient to express the size distribution with compact parameters, like the effective radius r_e and the effective number concentration N_e. The effective radius is directly linked to the extinction properties of the layer. These two quatities are defined as follows (see,

AMTD
8, 8439–8481, 2015

e.g., Korolev et al., 1999):

$$r_e = \frac{\int r^3 n(r) \mathrm{d}r}{\int r^2 n(r) \mathrm{d}r} \quad (2)$$

$$N_e = \frac{\left(\int r^2 n(r) \mathrm{d}r\right)^3}{\left(\int r^3 n(r) \mathrm{d}r\right)^2} \quad (3)$$

Because σ_r is fixed in our simulations, it follows that:

$$r_e = r_m e^{2.5 \ln^2 \sigma_r} = 2.619\, r_m \quad (4)$$

$$N_e = N_0 e^{-3.0 \ln^2 \sigma_r} = 0.315\, N_0 \quad (5)$$

The two quantities are defined in such a way that:

$$N_e r_e^2 = N_0 r_{surf}^2 \quad (6)$$

where $r_{surf} = \frac{1}{N_0} \int r^2 n(r) \mathrm{d}r$ is the mean surface area of the aerosol layer. Please find in Tables 1 and 2 the total number concentrations and the mean radii used in this work, with the corresponding effective radii and number concentrations.

Then, from these two quantities and the sulphate aerosols density, the effective mass volume concentration (in $\mathrm{g\,m^{-3}}$) can be defined as follows:

$$M_e = \frac{4}{3} \pi \rho(c) r_e^3 N_e \quad (7)$$

In Eq. (7), $\rho(c)$ is the density of the sulphate aerosols (a function of the H_2SO_4 concentration), which has been considered as fixed in a given aerosols layer. The effective mass volume concentration can then be used to calculate the total mass (in g, by multiplying by the volume occupied by the aerosols) or the effective columnar abundance

AMTD
8, 8439–8481, 2015

(in g m^{-2} by multiplying by the vertical altitude interval occupied by the aerosols). This latter quantity:

$$M_{\mathrm{col}} = M_{\mathrm{e}} \cdot \Delta z \tag{8}$$

is linked to the total absorption due to the presence of sulphate aerosols and is considered in the following discussions.

The extinction coefficient β_{ext}, discussed in the following sections, can be expressed as follows:

$$\begin{aligned}\beta_{\mathrm{ext}}(c, r_{\mathrm{e}}, N_{\mathrm{e}}, \nu) &= \int \pi r^2 Q_{\mathrm{ext}}(m(c), r, \nu) n(r) \mathrm{d}r \\ &= \int \pi r^2 Q_{\mathrm{ext}}(m(c), r, \nu) \frac{N_0}{r \ln \sigma_r \sqrt{2\pi}} e^{-\frac{1}{2}\left(\frac{\ln(r/r_{\mathrm{m}})}{\ln \sigma_r}\right)^2} \mathrm{d}r\end{aligned} \tag{9}$$

where $Q_{\mathrm{ext}}(m(c), r, \nu)$ is the single particle extinction efficiency factor from Mie theory, m is the complex refractive index, which is a function of the H_2SO_4 mixing ratio (c) and $n(r)$ is the considered log-normal size distribution. The mean radius and the total number concentration are linked to the effective radius and number concentration by Eqs. (4) and (5). The dependence of the β_{ext} spectra to c is transferred from Q_{ext}, and the dependence to N_{e} and r_{e} is transferred from $n(r)$. From the Eq. (9), it follows that the extinction coefficient can be separated in two factors:

$$\beta_{\mathrm{ext}}(c, r_{\mathrm{e}}, N_{\mathrm{e}}, \nu) = N_{\mathrm{e}} \mathrm{F}(c, r_{\mathrm{e}}, \nu) \tag{10}$$

where the function $F(c, r_{\mathrm{e}}, \nu)$ does not depend from the effective number concentration N_{e}.

AMTD
8, 8439–8481, 2015

3 Optical characterization of the sulphate aerosol layers: dependence of the extinction coefficient from chemical and micro-physical properties

3.1 Sulphate aerosols absorption and scattering

We first analyze the spectral extinction coefficient for different chemical and micro-physical properties of the sulphate aerosols layer. Previous studies on the retrieval of sulphate aerosols have neglected the scattering component of the extinction coefficient in the TIR spectral region, see, e.g., Griessbach et al. (2015). In Fig. 1 we show the single scattering albedo (the ratio of the scattering and the extinction coefficient) of sulphate layers with two different H_2SO_4 mixing ratios (64 and 75 %) and two typical size distributions: a background, volcanically-quiescent aerosol layer ($N_0 = 8\,cm^{-3}$, $r_m = 0.07\,\mu m$, $\sigma_m = 1.86$), and a moderately-perturbed volcanic aerosol layer ($N_0 = 20\,cm^{-3}$, $r_m = 0.3\,\mu m$, $\sigma_m = 1.86$). In volcanically-perturbed conditions, the number concentration N_0 is higher due to the enhanced formation of new particles from sulphur dioxide emissions and the mean radius r_m is bigger due to the enhanced coagulation of droplets in denser environments (see, e.g., McCormick et al., 1995; Deshler et al., 2003). In Fig. 1, as well as in the other figures of this section, the spectral discretization (available wavenumbers) originates from the spectral discretization of the refractive indexes in the database of Biermann et al. (2000). While the absorption dominates the extinction in the TIR spectral region, the scattering component has increasing values for bigger particles and can reach values up to about 20 % in volcanic conditions. This result suggests that the scattering component of the extinction, even if relatively small with respect to the absorption, cannot be neglected. Correspondingly, in the following sections we study the extinction coefficient of the layer. The parameters of the aerosol layer are the H_2SO_4 mixing ratio, the temperature and the size distribution.

AMTD
8, 8439–8481, 2015

3.2 Dependence of the extinction coefficient to the H_2SO_4 mixing ratio and the temperature

To study how the extinction of the layer varies with respect to the H_2SO_4 mixing ratio and the temperature, we use the tabulated combinations of mixing ratios and temperatures in GEISA, as described in Sect. 2, and we fix the size distribution. We consider the two size distributions, background and volcanic, introduced in Sect. 3.1. As said before, the absorption dominates over the scattering and then the extinction coefficient discussed in the following is mostly defined by the sulphate absorption spectral features, except for a small correction for layers with bigger particles (volcanic conditions).

Figure 2 shows the extinction coefficient in the range 600 to 1400 cm^{-1} for sulphate aerosol layers at temperatures of 293 and 213 K, and different H_2SO_4 mixing ratios, depending on the availability of mixing ratio/temperature combinations in the dataset. The complete dataset, for all available temperatures in the interval 188–293 K can be found in Figs. 1 and 2 of the Supplement. In all cases, the extinction in volcanically-perturbed conditions is at least 50 times larger than in non-volcanic conditions, as a result of more (N_0 = 20 vs. 8 cm^{-3}) and bigger (r_m = 0.3 vs. 0.06 µm) particles. This suggests a strong sensitivity of the sulphate aerosols extinction to the size distribution, which is more thoroughly discussed in Sect. 3.3. The H_2SO_4 mixing ratio is a relatively sensitive parameter as well, as the variability of the extinction coefficient with respect to this parameter is over a factor 3 to 5, for each given temperature. The sulphate absorption region is located in this spectral range and is clearly visible. A minimum extinction occurs at 650–800 cm^{-1}. Then, from 900 to 1300 cm^{-1} the absorption bands of the sulphate ion (ν_3 SO_4^{2-} asymmetric stretch band, centred at about 1104 cm^{-1}), the bisulphate ion (ν_1 SO_3^- symmetric stretch band, centred between 1030 and 1050 cm^{-1}) and of the undissociated sulphuric acid molecule (combination of bend and stretch of different groups, with absorption peaks centred at 905, 965 and 1170 cm^{-1}) dominate, generating a general increase with wavelength of the absorption (and then of the extinction) in this spectral region, with additional absorption features at smaller spectral

AMTD
8, 8439–8481, 2015

resolution. At mixing ratios larger than 50 % and all temperatures, a quite elevated maximum of the H_2SO_4 molecule absorption at 1170 cm^{-1} appears; for smaller mixing ratios and lower temperatures, the sulphate ion absorption feature at 1104 cm^{-1} dominates, while the impact of the H_2SO_4 molecular absorption at 1170 cm^{-1} is less marked. Two further peaks can be found at about 905 cm^{-1} (sulphuric acid molecular band) and 1050 cm^{-1} (bi-sulphate ion bands). In general, the H_2SO_4 absorption bands are more important for concentrated solutions (> 60 %), as Giguère and Savoie (1960) first noticed and attributed to different auto-dissociation equilibria occurring at such higher concentrations. For more diluted solutions, the dependence of the absorption spectra on temperature is due to the dependence of the dissociation constant of the sulphate/bisulphate system on temperature (Biermann et al., 2000). Except for this effect, the temperature seems a much less important factor than the mixing ratio, to determine the absorption properties of the aerosol layer, especially in *real world* UTLS conditions (H_2SO_4 mixing ratios greater than 60 %, temperatures smaller than 220 K SPARC, 2006).

A general increasing absorption by UTLS secondary sulphate aerosols in the range 700–1300 cm^{-1} has been indeed observed in the past by satellite limb observations, due to the Mount Pinatubo eruption of 1991 (Grainger et al., 1993). The two absorption peaks at 905 and 1170 cm^{-1} have also been observed by MIPAS-B (Michelson Interferometer for Passive Atmospheric Sounding – Balloon-borne version) limb observations, at altitudes between 11 and 16 km, for the same volcanic event (see the spectra of Fig. 3 in Echle et al., 1998, which has shapes and absolute values comparable to those of Fig. 2 of the present paper, for volcanic conditions, higher H_2SO_4 mixing ratios and temperatures of about 200 K). Nevertheless, Grainger et al. (1993) and Echle et al. (1998) did not explicitly relate the observed absorption coefficient spectra to these specific molecular H_2SO_4 vibration modes.

To further demonstrate the very small sensitivity of the sulphate extinction spectra to temperature, and the much more important contribution of the H_2SO_4 mixing ratio, we made a linear regression of the maximum extinction at 1170 cm^{-1} and its ratio

AMTD
8, 8439–8481, 2015

to the minimum extinction near 800 cm^{-1}, as a function of the temperature, at fixed mixing ratios (parameters of the regressions in Tables 1 and 2 in the Supplement), for background and volcanically-enhanced situations. In general, the extinction does not vary much with temperature, except for a few cases, e.g., a 20 % variation of the absolute extinction, from 183 to 293 K, with a mixing ratio of 57 % in both background and volcanic conditions. For other mixing ratios, the variation with temperature is less than 10 %. This variability is much more limited than that due to mixing ratio variations, which can be larger than 100 % (for example, the maximum absorption at 1170 cm^{-1} varies from about 2.5×10^{-3} to about 6.0×10^{-3} km^{-1}, and from about 2.5×10^{-5} to about 6.0×10^{-5} km^{-1}, in volcanic and background conditions, respectively, with mixing ratios spanning 30 to 64 %). The variability of the relative extinction 1170–800 cm^{-1} with temperature is even smaller.

These analyses of the dependence of the extinction coefficient on the temperature and H_2SO_4 mixing ratio point out that the temperature of the aerosol layer (and then its altitude) cannot be retrieved from aerosol extinction measurements, especially for mixing ratios greater than 60 %. From a different perspective, this is beneficial for the retrieval of sulphate aerosol chemical and micro-physical parameters because this property limits the number of sensitive factors affecting the extinction spectra variability. The extinction, and more in particular the absorption signature, are very sensitive to the H_2SO_4 mixing ratio of the binary solution H_2SO_4/H_2O, both in background and volcanically-enhanced situations, paving the way to a retrieval.

3.3 Dependence of the extinction coefficient from the size distribution

Figure 2 suggests that the sulphate extinction signature is sensitive to the size distribution of the aerosol layer. In this section, we systematically investigate this dependence by estimating the individual contributions of the number concentration and effective radius. To conduct targeted analyses on the UTLS sulphate aerosols, we have limited the H_2SO_4 mixing ratio to four values, 60, 64, 70 and 75 %, and the temperature to two

AMTD
8, 8439–8481, 2015

close values, 213 and 215 K, among those available in the database. This is intended to simulate typical tropical UTLS temperatures (see, e.g., Lamsal et al., 2004) and typical mixing ratios within dehydrated atmospheric regions (SPARC, 2006).

Figure 3a and b shows the extinction coefficient in the spectral range 600–1400 cm^{-1}, for these UTLS conditions, as a function of the effective number concentration N_e, illustrating the proportionality shown in Eq. (10). The range of variation of N_e (see Table 2) covers from background to severe volcanic conditions. The effective radius r_e (corresponding r_m in parentheses) is fixed at 0.79 (0.30) µm. The H_2SO_4 mixing ratio is fixed at 60 % (a) and 75 % (b). Figure 3c and d shows the extinction coefficient in the spectral range 600–1400 cm^{-1} as a function of the effective radius r_e. Note that in this figure the ordinate axis is logarithmic, to better show the spectral behaviour of the different curves. The effective number concentration N_e (corresponding N_0 in parentheses) is now fixed at 7.87 (20.00) cm^{-3}. The H_2SO_4 mixing ratio is fixed at 60 % (c) and 75 % (d). The spectral patterns of the sulphate/bi-sulphate ions and the sulphuric acid molecule are clearly visible for all effective number concentrations and radii, with the same 3 marked peaks that emerged in Fig. 2. Figure 3c and d shows that $F(c, r_e, \nu)$ depends strongly on r_e, growing monotoneously with r_e. The growth is not, however, uniform in ν, as spectral extinction gets flatter with bigger sulphate particles. In general, the extinction is very small for smaller particles. Comparing Fig. 3a, b and 3a, c, it appears that the most important condition leading to significant extinction is a large effective radius of the layer. At fixed H_2SO_4 mixing ratio, the variability of the extinction, e.g., at the maximum aborption at 1170 cm^{-1}, due to the effective radius can be up to 2 orders magnitude stronger than that due to the effective number concentration.

3.4 Discussion on sulphate aerosols extinction

The spectral extinction of sulphate aerosol layers is, to different extents, sensitive to the three chemical and micro-physical parameters under investigation, namely the H_2SO_4 mixing ratio, the effective radius and the effective number concentration.

AMTD
8, 8439–8481, 2015

In Sects. 3.2 and 3.3 we have analyzed the dependence of the spectral extinction curves as a whole, in function of the chemical and micro-physical properties: H_2SO_4 mixing ratio, the effective radius and the effective number concentration. We now fix the wavenumber. At a selected wavenumber $\bar{\nu}$ the extinction coefficient AE (absolute extinction) is (see Eq. 10):

$$\mathrm{AE} = \beta_{\mathrm{ext}}(c, r_{\mathrm{e}}, N_{\mathrm{e}}, \bar{\nu}) = N_{\mathrm{e}}\mathrm{F}(c, r_{\mathrm{e}}, \bar{\nu}) \tag{11}$$

We introduce the ratio RE (relative extinction) between the extinction coefficient at two different wavenumbers ν_1 and ν_2:

$$\mathrm{RE} = \frac{\beta_{\mathrm{ext}}(c, r_{\mathrm{e}}, N_{\mathrm{e}}, \nu_1)}{\beta_{\mathrm{ext}}(c, r_{\mathrm{e}}, N_{\mathrm{e},\nu_2})} = \frac{N_{\mathrm{e}}\mathrm{F}(c, r_{\mathrm{e}}, \nu_1)}{N_{\mathrm{e}}\mathrm{F}(c, r_{\mathrm{e}}, \nu_2)} = \mathrm{G}(c, r_{\mathrm{e}}, \nu_1, \nu_2) \tag{12}$$

The two functions $\mathrm{F}(c, r_{\mathrm{e}}, \bar{\nu})$ and $\mathrm{G}(c, r_{\mathrm{e}}, \nu_1, \nu_2)$, and then AE and RE, depend on the choice of the wavenumbers $\bar{\nu}$, ν_1 and ν_2. The absolute and relative extinction at selected wavenumbers are important for remote sensing applications, in particular for radiometers that have broad-band channels at a number of wavenumbers. Here we select specific wavenumbers where informative features of the spectral extinction of sulphate aerosol layers are found, as discussed in Sects. 3.2 and 3.3. Correspondigly, we introduce three spectral quantities: the maximum AE at 1170 cm^{-1} (hereafter referred to as ME, maximum extinction), (2) its relative extinction with respect to the minimum extinction at 800 cm^{-1} (the extinction ratio between 1170 and 800 cm^{-1}, hereafter referred to as RE1), (3) the relative extinction of the secondary peak at 905 cm^{-1} with respect to the minimum extinction at 800 cm^{-1} (the extinction ratio between 905 and 800 cm^{-1}, hereafter referred to as RE2). We recall that the extinction peaks at 1170 and 905 cm^{-1} are mostly due to molecular H_2SO_4 absorption bands. Another important spectral feature in the sulphate signature is the extinction peak due to the ionic absorption at 1050 cm^{-1}, but we exclude this latter because the information in this band is disturbed by the ozone absorption band region at 9.6 µm (more details in Sect. 5).

AMTD
8, 8439–8481, 2015

The variability of the spectral parameter ME as a function of the H_2SO_4 mixing ratio and effective radius and number concentration has been discussed in Sect. 3.3. As it can be seen from Fig. 3, ME varies between near-zero values (for small N_e, r_e and c) and 40×10^{-3} km^{-1} (large values of the three aerosol parameters). ME is very small for small effective radii, unregarding the value of the effective number concentration and H_2SO_4 mixing ratio. Higher values ($> 10 \times 10^{-3}$) are only found for effective radii bigger than about 0.5 µm. This is an indication of the small sensitivity of the spectral extinction to sulphate aerosols in background conditions, and the dominating role of the particle size in ME, and then in the depth and the whole curve of the sulphate spectral extinction signature. Figure 4a, b shows the variability of the spectral parameters RE1 and RE2 as a function of effective radius and H_2SO_4 mixing ratio, as RE1 and RE2 are independent from the effective number concentration (see Eq. 12). The behaviour of RE1 and RE2 is similar, with increasing values for higher H_2SO_4 mixing ratios and smaller particles.

As both RE1 and RE2 depend on c and r_e but not on N_e, it is useful to determine whether they differ in this dependency, having in mind the possibility to retrieve c and r_e from spectrometric measurements. Figure 4c shows the angle of the gradients of RE1 and RE2 with respect to c and r_e normalized to vary over the same range. If the angle is near-zero, the gradients are parallel vectors and then the variations of RE1 and RE2 carry a very dependent information content. Conversely, for angles departing from zero the information content about the aerosol parameters is more and more independent. It is visible that the angle remains small for small r_e and when both r_e and c are large, and that there is an optimal sensitivity range which more or less extends about a diagonal from the upper left of the diagram, with angles between 15 and 30°.

To conclude this section, we suggest that the use of these three spectral parameters, ME, RE1 and RE2 could be used to detect and extract some quantitative information on UTLS sulphate aerosols, in the case of volcanically-enhanced conditions. ME is sensitive to the three aerosol parameters, while RE1 and RE2 are only sensitive to the H_2SO_4 mixing ratio and the effective radius. In principle, the information content

AMTD
8, 8439–8481, 2015

carried by ME, RE1 and RE2 on the H_2SO_4 mixing ratio, effective radius and number concentration is partially independent for most conditions and then broad-band retrieval schemes could be developped using these three spectral parameters. One option could be to infer the H_2SO_4 mixing ratio and the effective radius from RE1 and RE2, and then use this information to derive the number concentration with ME1. In practice, due to the partial correlation of the information content of RE1 and RE2 on the H_2SO_4 mixing ratio and the effective radius, and the scarce sensitivity of ME to the effective number concentration for background non-volcanic conditions, the sulphate aerosol parameters might be hardly retrievable at those conditions. On the other hand, in volcanically-enhanced conditions there is an enhanced variability of ME with respect to the three aerosol parameters but the variability of RE1 and RE2 with respect to the H_2SO_4 mixing ratio is relatively small, and the correlation of their information content is high for bigger values of the H_2SO_4 mixing ratio. All these considerations suggest that the three aerosol parameters are retrievable as independent quantities only for limited conditions, when using broad-band sulphates extinction spectral features and contraints should be given to at least one parameter (e.g., the effective number concentration). The approach of using absolute and relative extinction features is applicable to both high-resolution and broad-band TIR satellite sensors as MODIS (Moderate Resolution Imaging Spectroradiometer) (Barnes et al., 1998) or SEVIRI (Spinning Enhanced Visible and InfraRed Imager), even if these latter instruments may not have optimized channels for sulphate aerosols observations.

4 Spectral sensitivity of IASI pseudo-observations to chemical and micro-physical properties

In order to test the sensitivity of satellite nadir observation in the TIR to sulphate aerosols and the perturbation brought by other atmospheric species under real conditions, the spectral extinction coefficients of the sulphate aerosol layers obtained in Sect. 3 are here used as inputs of the forward radiative transfer modelling described

AMTD
8, 8439–8481, 2015

in Sect. 2. As done for Sects. 3.3 and 3.4, we restrict our attention to H_2SO_4 mixing ratios of 60, 64, 70 and 75 % and temperature of the droplets of 213–215 K, within the set of tabulated values. As demonstrated in Sect. 3.2, the extinction properties of the H_2SO_4/H_2O droplets layers are very weakly dependent on the temperature. The chosen parameters are intended to mimic a realistic tropical UTLS situation, given the constrains of our dataset. The altitude of the sulphate aerosol layer has been fixed at about 150 hPa. A typical tropical atmosphere (temperature, humidity and gas concentration profiles) is selected from those available in 4A/OP. Then we conduct 256 simulations by varying the four H_2SO_4 mixing ratio/temperature combinations and all the available effective number concentrations and effective radii (see Tables 2 and 1). A further simulation is made with the same atmosphere but without a sulphate aerosol layer, to define a baseline and to isolate the sulphate aerosol impact on the output spectra. Finally, 256+1 IASI spectral BT pseudo-observations are obtained. We then define a sulphate aerosol brightness temperature signature (hereafter simply referred to as *BT signature*) as the spectral differences between each of the 256 brightness temperature spectra and the one obtained with the baseline run. Figure 5 shows examples of BT signatures for different combinations of the effective number concentration, the effective radius and the H_2SO_4 mixing ratio. In the spectral region 700–1300 cm^{-1} a few main interfering features emerge, like the ubiquitous weak absorption bands of H_2O and the strong rotational-vibrational ozone band centred at 9.6 µm (1041.67 cm^{-1}) and affecting the spectral region of approximately 980–1080 cm^{-1} (see also Fig. 8). A first evidence is that the signal of the bi-sulphate ion bands at 1030 and 1050 µm is completely lost because of the interference with the ozone band. This justifies discarding these absorption features in the discussion of Sect. 3.4. The sulphate ion band at 1104 cm^{-1} and the weaker bi-sulphate band at 965 cm^{-1} are partially also affected by the peripheral region of the ozone band. Therefore, it is impossible to use the ionic bands to infer useful information on sulphate aerosols. This is mostly unconvenient for small mixing ratios, where ionic absorption dominates over molecular absorption (see Fig. 2). On the contrary, the molecular H_2SO_4 absorption band at 1170 cm^{-1}, as

AMTD
8, 8439–8481, 2015

well as the weaker H_2SO_4 band at 905 cm^{-1} and the background region at 800 cm^{-1} are clearly visible, while still partly affected by the weak, fine scale, ubiquitous water absorption lines.

The stronger band at 1170 cm^{-1} is the most important feature in the sulphate aerosol extinction spectra and is responsible of the typical "increasing extinction" or "decreasing BT signature" shape between 700 and 1200 cm^{-1}, which has been empirically observed in the past (see, e.g., Grainger et al., 1993; Echle et al., 1998; Clarisse et al., 2010; Griessbach et al., 2015). In Sect. 3 it was found that the extinction signature of the sulphate aerosols, and the three partially-independent spectral parameters ME, RE1 and RE2 are sensitive to the H_2SO_4 mixing ratio and to the size distribution, and this sensitivity is dominated by the effective radius. Consistently, from Fig. 5 it can be seen that the depth of the BT signature (and then ME) is strongly dependent on the effective radius and much less sensitive to the effective number concentration and the H_2SO_4 mixing ratio. However, for fixed effective radius and number concentration, there is a variation of the spectral slope between 700 and 1200 cm^{-1} with the H_2SO_4 mixing ratio. This is again consistent with the results of Sect. 3.4. In general, the BT signatures at 1170 cm^{-1} are less than 0.7 K for small particles, with effective radii smaller than 0.52 µm, for all number concentration and H_2SO_4 mixing ratio. The BT signatures at 1170 cm^{-1} can reach values of 3.0 to 5.0 K for bigger particles, with higher values for larger number concentration and H_2SO_4 mixing ratio. Values of r_e of 0.6–0.7 µm and higher are typical of coagulation effects in more or less severe volcanically-enhanced conditions. Thus, it seems very arduous to observe the background sulphate aerosol layers, while BT signatures of volcanic sulphates can be relatively strong.

The variability of the spectral BT signature with effective number concentration, effective radius and H_2SO_4 mixing ratio is more systematically displayed in Fig. 6. This figure shows the BT signature in the spectral range 700–1300 cm^{-1}, as a function of the effective number concentration N_e, for a fixed effective radius r_e = 0.79 µm, and as a function of the effective radius r_e, for a fixed effective number concentration N_e = 7,87 particles cm^{-3}. The same patterns evidenced in Fig. 5, the discussion above

AMTD
8, 8439–8481, 2015

and the results of Sect. 3, are systematically observed in these plots. A marked maximum of the BT signature at 1170 cm^{-1} as well as secondary maximum at 905 cm^{-1}, both due to the molecular H_2SO_4 absorption, are apparent. The dramatic difference for Fig. 6c and d from smaller to bigger effective radii, is a confirmation of the relative importance of the effective radius in determining the signature of the UTLS sulphate aerosols in TIR spectra, and the very low sensitivity at background conditions.

The analyses of the present Section, in conjunction with the discussion of Sect. 3.4, suggest that information on chemical and micro-physical properties of sulphate aerosols can be extracted using broad band spectral features, e.g., the maximum absorption near 1170 cm^{-1}, and the spectral ratios between 1170 and 800 cm^{-1} and between 905 and 800 cm^{-1}. Nevertheless, the presence of relatively well separated ionic and molecular absorption signatures justify the use of a spectral fitting approach to extract the full information content using finer specral resolution. These fine scale structures are typical of liquid aerosols. Thus, we wish to stress how high spectral resolution observations, like those made by IASI, can bring a significant added-value in the characterization of such aerosols.

5 Interferring parameters

5.1 Interference with temperature and humidity profiles variability

We consider here how uncertainties in the temperature and humidity profile may mask the sensitivity to sulphate aerosols. The TIGR (Thermodynamic Initial Guess Retrieval) database is a library of 2311 representative atmospheric situations (tropical, mid-latitude and polar) selected by statistical methods from an ensemble of 80 000 radiosonde measurements (Chédin et al., 1985; Chevallier et al., 1998). We have calculated the average temperature and water vapour mixing ratio profile from TIGR. Only the tropical atmosphere situations (872 profiles) have been considered. Figure 7a and b shows the individual tropical temperature and water vapour profiles, respectively,

AMTD
8, 8439–8481, 2015

and the average profiles with standard deviations. We then generate two datasets of 128 profiles each, by perturbing the average temperature (one set of 128 perturbed profiles) and water vapour profile (one set of 128 perturbed profiles) with a height-dependent Gaussian noise. For each level, we added a random value from a Gaussian distribution of zero-mean-value and variable standard deviation, depending on the altitude level, to simulate the actual temperature and water vapour retrieval uncertainties of IASI, as estimated, e.g., by Pougatchev et al. (2009). In this latter work, temperature and water vapour profiles uncertainties are estimated by comparing a dataset of IASI temperature and water vapour profile retrievals with co-located radiosonde profiles. The standard deviations of the Gaussian perturbation are assumed between 0.5 and 2.0 K (temperature) and between 3 and 10 % (water vapour mixing ratio), as shown in Fig. 7a and b, respectively. We then performed two sets of 128 4A/OP forward radiative transfer runs with: (1) the average temperature profile and the 128 perturbed water vapour profiles (H_2O-perturbed runs), (2) the average water vapour profile and the 128 perturbed temperature profile (T-perturbed runs), and a further run with average temperature and water vapour profiles (baseline run for this analysis). For these runs, the sulphate aerosol layer size distribution and chemical composition has been taken fixed at moderate volcanic conditions (log-normal distribution with: $N_0 = 20\,\mathrm{cm}^{-3}$, $r_m = 0.2\,\mu\mathrm{m}$, $\sigma_m = 1.86\,\mu\mathrm{m}$, 70 % H_2SO_4 mixing ratio) at about 150 hPa altitude. Two sets of spectral differences are finally calculated: a first set of differences between the T-perturbed and the baseline runs, and a second set of differences between the H_2O-perturbed and the baseline runs. Figure 7c shows the mean values of T-perturbed minus baseline, and H_2O-perturbed minus baseline differences and spectral variability (represented by its 1-standard deviation interval) of these differences.

The temperature profile uncertainties dominate the spectral brightness temperature variability, with a sensitivity up to ±1.4 K, peaking in the sulphate-sensitive spectral region between 1100 and 1200 cm^{-1}, while the impact of water vapour concentration profile uncertainties is generally smaller than ±0.2 K. The broad-band magnitude of these fluctations indicates a further limitation on the observation of sulphate aerosol

AMTD
8, 8439–8481, 2015

chemical and micro-physical properties in non-volcanically perturbed conditions with IASI-like instruments, at least for BT sulphates signatures smaller than about 2.0 K (see Fig. 5). At a smaller spectral resolution, it is clear that the regions characterized by water vapour absorption lines must be avoided by a careful selection of the spectral micro-windows of the retrieval algorithm.

The previous analysis was aimed at the evaluation of the impact of temperature and humidity profiles uncertitudes when these quantities are retrieved with the same TIR observations used to infer the sulphate aerosols properties. This discussion is then of interest when considering near-real time multi-parameter retrievals. In offline retrieval schemes, temperature and humidity profiles can be taken from model reanalyses. It must be noted that these profiles have significanty smaller uncertainties than profiles obtained with TIR observations, then in these cases their impact on the retrieval of sulphate aerosols is more limited.

5.2 Other interferring species: SO_2, CO_2 and ash

In the TIR spectral region where sulphate aerosols have their absorption features (700–1300 cm^{-1}), other gaseous species have absorption bands, which can interfer with the sulphate BT signature. Figure 8 shows the absorption cross sections of water vapour, carbon dioxide, ozone and sulphur dioxide in this spectral range. As discussed in Sects. 4 and 5.1, the water vapour lines are ubiquitous and must be taken into account when selecting the spectral micro-windows of a retrieval algorithm; at the same time, the ozone band perturbs the region between about 980 and 1080 cm^{-1}, thus preventing from using the sulphate ions bands around 1050 cm^{-1}. The sulphur dioxide absorption bands lie in the range 1080–1230 cm^{-1} and then can partially affect the maximum sulphate absorption region around 1170 cm^{-1}. The use of high-resolution TIR spectrometers, like IASI, is then recommandable to select targeted spectral micro-windows to minimize the effect of the sulphur dioxide interferrence, e.g., around 1150 cm^{-1}. The carbon dioxide bands are stronger for wavenumbers less then about 750 cm^{-1}, and then of lower concern for the present study. It is interesting to note that enhanced con-

AMTD
8, 8439–8481, 2015

centrations of sulphur dioxide, carbon dioxide and water vapour are co-existent with sulphate aerosols in volcanic plumes, where the the sulphate BT signature is stronger.

Another important volcanic effluent that has a spectral signature in the range 700–1300 cm^{-1} is the ash. The ash BT signature has a typical V shape in this range, as shown, e.g., by Dubuisson et al. (2014) and Clarisse et al. (2010), which can be modulated by its mineralogical composition (Dubuisson et al., 2014) and optical depth (Corradini et al., 2009). This ash BT signature is characterized by a stronger absorption at about 950–1100 cm^{-1} than at longer (1200 cm^{-1}) and shorter wavenumbers (850 cm^{-1}), as shown in Fig. 1b of (Clarisse et al., 2010). In Fig. 9 the impact of different UTLS sulphate aerosol layers on the top of the atmosphere (TOA) radiance spectra, as for our simulations, is shown. The spectra are expressed in radiance units as a function of the wavelength to more readily compare the impact of the sulphate absorption to the impact of ash, as reported in Fig. 1 of (Corradini et al., 2009). The reduction of the TOA radiance due to ash is typically 10 to 25 % at its maximum absorption spectral range (about 10–11 µm, 1000–910 cm^{-1}), depending on the ash optical depth. Sulphates can impact for a few percent, for small and diluted droplets (green lines in Fig. 9), to up to about 25 % for volcanically-enhanced conditions (red lines in Fig. 9) at its maximum extinction spectral range (about 8.5–9.0 µm, 1175–1110 cm^{-1}). As pointed out by Clarisse et al. (2010), the different shapes of the ash and sulphate absorption signatures facilitate the discrimination of the two different aerosol particles. In addition, in extreme volcanic conditions, the magnitude of the sulphate signature is comparable to that of ash. The comparison of Figs. 9 and 1 of (Corradini et al., 2009) permits as well the comparison of the impact of sulphate aerosols and that of sulphur dioxide absorptions on the TOA radiances. This latter is generally a few percent, with a maximum at about 9 µm (1110 cm^{-1}), and then comparable to the sulphate aerosol impact for background to moderate volcanic conditions.

AMTD
8, 8439–8481, 2015

6 Conclusions

In this paper we have presented sensitivity analyses on the optical properties and BT signatures of secondary sulphate aerosols in the UTLS, based on TIR IASI pseudo-observations obtained with the 4A/OP radiative transfer model. We have modelled the sulphate aerosols as layers of H_2O/H_2SO_4 binary solution droplets with varying temperatures, mixing ratios and size distributions. The optical properties of these layers are obtained with a Mie code, taking as inputs the complex refractive indexes of H_2O/H_2SO_4 bynary solution with different temperatures and H_2SO_4 mixing ratios from laboratory measurements and archived in the GEISA database, and size distribution with different effective radii and effective number concentrations.

For these layers, we have determined characteristic BT spectral signatures in the spectral range 700–1200 cm^{-1}, due to sulphate and bi-sulphate ions, and molecular undissociated H_2SO_4 absorption bands in the TIR. In this spectral region, a general decreasing BT signature (increasingly negative difference with respect to a no-aerosols baseline due to the increasing extinction coefficient) is observed. This signature is dominated by the stronger molecular H_2SO_4 absorption band at 1170 cm^{-1}, which is particularly pronounced for realistic tropical UTLS conditions (low temperatures and H_2SO_4 mixing ratios greater than 60 %). The BT signature can reach values as high as −5.0 K at 1170 cm^{-1}, for big particles, and high number concentration and H_2SO_4 mixing ratio. These conditions are typical of a volcanically perturbed UTLS. Another important feature that can modulate the shape of the BT sulphate aerosol signature is the H_2SO_4 absorption band at 905 cm^{-1}. The extinction of the aerosol layer is found very weakly sensitive to the temperature of the droplets. The spectral extinction and then the BT signature is, at different extents, sensitive to the H_2SO_4 mixing ratio, the effective radius and number concentration. In general, the effective radius qualifies as the dominating factor determining the sensitivity of the sulphate aerosols extinction spectra and BT signatures. Sulphate aerosol layers in background conditions (small H_2SO_4 mixing ratios, and number concentrations and effective radii) seem not observable by IASI-like

AMTD
8, 8439–8481, 2015

TIR instruments because of (1) small BT signatures, mainly due to the high sensitivity to the effective radius, and (2) the interference of the 9.6 µm ozone absorption band, which is superposed to the main sulphate/bi-sulphate ion absorption bands. BT spectral variability induced by the uncertainties on the vertical temperature profile and surface temperature are a further limiting factor for the observation of chemical and micro-physical parameters of background sulphate aerosol layers in the UTLS. Other interferring species are identified, like sulphur dioxide, carbon dioxide, water vapour and ash. While carbon dioxide absorption bands are of limited concern in this context (stronger impact for wavenumebers lower than about 750 cm^{-1}), attention must be paid to the sulphur dioxide absorption signature, which lies in the region of maximum sulphate BT signature, and the ubiquitous water vapour lines. The ash has a different BT signature than sulphates and its impact on the TOA radiances has a comparable magnitude to the volcanically-enhanced sulphate aerosols layers.

From a remote sensing perspective, these analyses show that broad-band features can be identified, like the maximum extinction at 1170 cm^{-1} (ME), its ratio with respect to the minimum extinction at 800 cm^{-1} (RE1) and the ratio of the secondary peak at 905 cm^{-1} with respect to the minimum extinction at 800 cm^{-1} (RE2). ME is sensitive to the H_2SO_4 mixing ratio, effective number concentration and radius, while RE1 and RE2 are only sensitive to the H_2SO_4 mixing ratio and the effective radius. While the information content carried by ME, RE1 and RE2 on the three aerosol parameters is partially independent for most conditions: (1) in background conditions ME is scarcely sensitive to the effective number concentration, and (2) in volcanically-enhanced conditions the variability of RE1 and RE2 with respect to the H_2SO_4 mixing ratio is very scarce, and the correlation of their information content is higher for higher H_2SO_4 mixing ratio. Then, with this broad-band approach the three aerosol parameters are hardly retrievable as independent quantities and contraints should be given to at least one parameter. Even if these broad-band spectral features are appealing to quantitatively characterize sulphate aerosols, an important factor for a better characterization is a fine spectral resolution. This is two-fold beneficial: (1) in a broad-band perspective, to ac-

AMTD
8, 8439–8481, 2015

curately select spectral micro-windows representing ME, RE1 and RE2 or other equivalent spectral parameters (dedicated channels not always available in moderate resolution instruments, like MODIS or SEVIRI), and free from water vapour, sulphur dioxide and ozone interference, (2) in a high spectral resolution spectral fitting perspective, to resolve the concurrent spectral absoption features of sulphates present in the aerosol droplets, and to precisely estimate the interferring parameters, as the temperature and humidity profile. A significant added-value is then expected from the forthcoming new generation of satellite TIR instruments, including IASI-NG (New Generation) that will be launched in the 2020 timeframe as part of the EPS-SG (EUMETSAT Polar System-Second Generation, formerly post-EPS) mission (Crevoisier et al., 2014).

The Supplement related to this article is available online at doi:10.5194/amtd-8-8439-2015-supplement.

Acknowledgements. The optical parameters of sulphate aerosols layers used in this work are obtained with the IDL Mie scattering routines developed by the Earth Observation Data Group of the Department of Physics of Oxford University, and available via the following website: http://eodg.atm.ox.ac.uk/MIE/. NOVELTIS is gratefully acknowledged for the support with the 4A/OP model. Alain Chédin, Virginie Capelle and Cyril Crevoisier are gratefully acknowledged for the help with 4A/OP, TIGR and the GEISA database. Hervé Herbin is gratefully acknowledge for the stimulating discussion during the last few years. This project has been partially supported by the EU 7th Framework Program under the grant 603557 (StratoClim).

References

Barnes, W., Pagano, T., and Salomonson, V.: Prelaunch characteristics of the Moderate Resolution Imaging Spectroradiometer (MODIS) on EOS-AM1, IEEE T. Geosci. Remote, 36, 1088–1100, doi:10.1109/36.700993, 1998. 8456

AMTD
8, 8439–8481, 2015

Bauman, J. J., Russell, P. B., Geller, M. A., and Hamill, P.: A stratospheric aerosol climatology from SAGE II and CLAES measurements: 1. Methodology, J. Geophys. Res.-Atmos., 108, 4382, doi:10.1029/2002JD002992, 2003. 8441

Biermann, U. M., Luo, B. P., and Peter, T.: Absorption spectra and optical constants of binary and ternary solutions of H_2SO_4, HNO_3, and H_2O in the mid infrared at atmospheric temperatures, J. Phys. Chem.-US, 104, 783–793, doi:10.1021/jp992349i, 2000. 8442, 8445, 8449, 8451, 8474

Boer, G. J., Sokolik, I. N., and Martin, S. T.: Infrared optical constants of aqueous sulfate–nitrate–ammonium multi-component tropospheric aerosols from attenuated total reflectance measurements: Part II. An examination of mixing rules, J. Quant. Spectrosc. Ra., 108, 39–53, doi:10.1016/j.jqsrt.2007.02.018, 2007. 8445

Bourassa, A. E., Degenstein, D. A., Elash, B. J., and Llewellyn, E. J.: Evolution of the stratospheric aerosol enhancement following the eruptions of Okmok and Kasatochi: Odin-OSIRIS measurements, J. Geophys. Res.-Atmos., 115, D00L03, doi:10.1029/2009JD013274, 2010. 8441

Chédin, A., Scott, N. A., Wahiche, C., and Moulinier, P.: Improved initialization inversion method: a high-resolution physical method for temperature retrievals from satellites of the TIROS-N series, J. Clim. Appl. Meteorol., 24, 128–143, 1985. 8459

Chevallier, F., Chéruy, F., Scott, N. A., and Chédin, A.: A neural network approach for a fast and accurate computation of a longwave radiative budget, J. Appl. Meteorol., 37, 1385–1397, doi:10.1175/1520-0450(1998)037<1385:ANNAFA>2.0.CO;2, 1998. 8459

Clarisse, L., Hurtmans, D., Prata, A. J., Karagulian, F., Clerbaux, C., Mazière, M. D., and Coheur, P.-F.: Retrieving radius, concentration, optical depth, and mass of different types of aerosols from high-resolution infrared nadir spectra, Appl. Optics, 49, 3713–3722, doi:10.1364/AO.49.003713, 2010. 8458, 8462

Clarisse, L., Coheur, P.-F., Prata, F., Hadji-Lazaro, J., Hurtmans, D., and Clerbaux, C.: A unified approach to infrared aerosol remote sensing and type specification, Atmos. Chem. Phys., 13, 2195–2221, doi:10.5194/acp-13-2195-2013, 2013. 8442

Corradini, S., Merucci, L., and Prata, A. J.: Retrieval of SO_2 from thermal infrared satellite measurements: correction procedures for the effects of volcanic ash, Atmos. Meas. Tech., 2, 177–191, doi:10.5194/amt-2-177-2009, 2009. 8462, 8481

Crevoisier, C., Clerbaux, C., Guidard, V., Phulpin, T., Armante, R., Barret, B., Camy-Peyret, C., Chaboureau, J.-P., Coheur, P.-F., Crépeau, L., Dufour, G., Labonnote, L., Lavanant, L., Hadji-

AMTD
8, 8439–8481, 2015

Lazaro, J., Herbin, H., Jacquinet-Husson, N., Payan, S., Péquignot, E., Pierangelo, C., Sellitto, P., and Stubenrauch, C.: Towards IASI-New Generation (IASI-NG): impact of improved spectral resolution and radiometric noise on the retrieval of thermodynamic, chemistry and climate variables, Atmos. Meas. Tech., 7, 4367–4385, doi:10.5194/amt-7-4367-2014, 2014. 8465

Deshler, T., Hervig, M. E., Hofmann, D. J., Rosen, J. M., and Liley, J. B.: Thirty years of in situ stratospheric aerosol size distribution measurements from Laramie, Wyoming (41°N), using balloon-borne instruments, J. Geophys. Res.-Atmos., 108, 4167, doi:10.1029/2002JD002514, 2003. 8446, 8449

Doeringer, D., Eldering, A., Boone, C. D., González Abad, G., and Bernath, P. F.: Observation of sulfate aerosols and SO_2 from the Sarychev volcanic eruption using data from the Atmospheric Chemistry Experiment (ACE), J. Geophys. Res.-Atmos., 117, D03203, doi:10.1029/2011JD016556, 2012. 8441

Dubuisson, P., Herbin, H., Minvielle, F., Compiègne, M., Thieuleux, F., Parol, F., and Pelon, J.: Remote sensing of volcanic ash plumes from thermal infrared: a case study analysis from SEVIRI, MODIS and IASI instruments, Atmos. Meas. Tech., 7, 359–371, doi:10.5194/amt-7-359-2014, 2014. 8462

Echle, G., von Clarmann, T., and Oelhaf, H.: Optical and microphysical parameters of the Mt. Pinatubo aerosol as determined from MIPAS-B mid-IR limb emission spectra, J. Geophys. Res.-Atmos., 103, 19193–19211, doi:10.1029/98JD01363, 1998. 8441, 8451, 8458

Eldering, A., Kahn, B. H., Mills, F. P., Irion, F. W., Steele, H. M., and Gunson, M. R.: Vertical profiles of aerosol volume from high spectral resolution infrared transmission measurements: results, J. Geophys. Res.-Atmos., 109, D20201, doi:10.1029/2004JD004623, 2004. 8441

Gettelman, A., Liu, X., Barahona, D., Lohmann, U., and Chen, C.: Climate impacts of ice nucleation, J. Geophys. Res.-Atmos., 117, D20201, doi:10.1029/2012JD017950, 2012. 8441

Giguère, P. A. and Savoie, R.: Les spectres infrarouges de l'acide sulfuriques et des oléums, Can. J. Chemistry, 38, 2467–2476, doi:10.1139/v60-334, 1960. 8451

Grainger, R. G., Lambert, A., Taylor, F. W., Remedios, J. J., Rodgers, C. D., Corney, M., and Kerridge, B. J.: Infrared absorption by volcanic stratospheric aerosols observed by ISAMS, Geophys. Res. Lett., 20, 1283–1286, doi:10.1029/93GL00823, 1993. 8441, 8442, 8451, 8458

AMTD
8, 8439–8481, 2015

Griessbach, S., Hoffmann, L., Spang, R., von Hobe, M., Müller, R., and Riese, M.: Infrared limb emission measurements of aerosol in the troposphere and stratosphere, Atmos. Meas. Tech. Discuss., 8, 4379–4412, doi:10.5194/amtd-8-4379-2015, 2015. 8449, 8458

Hamill, P., Jensen, E. J., Russell, P. B., and Bauman, J. J.: The life cycle of stratospheric aerosol particles, B. Am. Meteorol. Soc., 78, 1395–1410, doi:10.1175/1520-0477(1997)078<1395:TLCOSA>2.0.CO;2, 1997. 8441

Jacquinet-Husson, N., Scott, N. A., Chedin, A., and Chursi, A. A.: The GEISA spectroscopic database system revisited for IASI direct radiative transfer modelling, Atmospheric and Oceanic Optics, 16, 256–282, doi:10.1016/S0022-4073(02)00174-7, 2003. 8444

Jacquinet-Husson, N., Scott, N., Chédin, A., Crépeau, L., Armante, R., Capelle, V., Orphal, J., Coustenis, A., Boonne, C., Poulet-Crovisier, N., Barbe, A., Birk, M., Brown, L., Camy-Peyret, C., Claveau, C., Chance, K., Christidis, N., Clerbaux, C., Coheur, P., Dana, V., Daumont, L., Backer-Barilly, M. D., Lonardo, G. D., Flaud, J., Goldman, A., Hamdouni, A., Hess, M., Hurley, M., Jacquemart, D., Kleiner, I., Köpke, P., Mandin, J., Massie, S., Mikhailenko, S., Nemtchinov, V., Nikitin, A., Newnham, D., Perrin, A., Perevalov, V., Pinnock, S., Régalia-Jarlot, L., Rinsland, C., Rublev, A., Schreier, F., Schult, L., Smith, K., Tashkun, S., Teffo, J., Toth, R., Tyuterev, V., Auwera, J. V., Varanasi, P., and Wagner, G.: The {GEISA} spectroscopic database: current and future archive for Earth and planetary atmosphere studies, J. Quant. Spectrosc. Ra., 109, 1043–1059, doi:10.1016/j.jqsrt.2007.12.015, 2008. 8445

Kaufman, Y. J., Boucher, O., Tanré, D., Chin, M., Remer, L. A., and Takemura, T.: Aerosol anthropogenic component estimated from satellite data, Geophys. Res. Lett., 32, L17804, doi:10.1029/2005GL023125, 2005. 8442

Knopf, D. A., Koop, T., Luo, B. P., Weers, U. G., and Peter, T.: Homogeneous nucleation of NAD and NAT in liquid stratospheric aerosols: insufficient to explain denitrification, Atmos. Chem. Phys., 2, 207–214, doi:10.5194/acp-2-207-2002, 2002. 8445

Korolev, A. V., Isaac, G. A., Strapp, J. W., and Nevzorov, A. N.: In situ measurements of effective diameter and effective droplet number concentration, J. Geophys. Res.-Atmos., 104, 3993–4003, doi:10.1029/1998JD200071, 1999. 8447

Lamsal, L. N., Weber, M., Tellmann, S., and Burrows, J. P.: Ozone column classified climatology of ozone and temperature profiles based on ozonesonde and satellite data, J. Geophys. Res.-Atmos., 109, D20304, doi:10.1029/2004JD004680, 2004. 8453

AMTD
8, 8439–8481, 2015

McCormick, M. P., Thomason, L. W., and Trepte, C. R.: Atmospheric effects of the Mt Pinatubo eruption, Nature, 373, 399–404, doi:10.1038/373399a0, 1995. 8449

Miller, Y., Chaban, G. M., and Gerber, R. B.: Ab initio vibrational calculations for H_2SO_4 and $H_2SO_4 \times H_2O$: spectroscopy and the nature of the anharmonic couplings, J. Phys. Chem. A, 109, 6565–6574, doi:10.1021/jp058110l, 2005. 8445

Pougatchev, N., August, T., Calbet, X., Hultberg, T., Oduleye, O., Schlüssel, P., Stiller, B., Germain, K. St., and Bingham, G.: IASI temperature and water vapor retrievals – error assessment and validation, Atmos. Chem. Phys., 9, 6453–6458, doi:10.5194/acp-9-6453-2009, 2009. 8460

Remer, L. A., Kaufman, Y. J., Tanré, D., Mattoo, S., Chu, D. A., Martins, J. V., Li, R.-R., Ichoku, C., Levy, R. C., Kleidman, R. G., Eck, T. F., Vermote, E., and Holben, B. N.: The MODIS aerosol algorithm, products, and validation, J. Atmos. Sci., 62, 947–973, doi:10.1175/JAS3385.1, 2005. 8442

Robock, A. and Oppenheimer, C.: Volcanism and the Earth's Atmosphere, vol. 139 of Geophysical Monograph Series, American Geophysical Union, Washington, DC, USA, 2003. 8441

Scott, N. A. and Chedin, A.: A fast line-by-line method for atmospheric absorption computations: the automatized atmospheric absorption atlas, J. Appl. Meteorol., 20, 802–812, doi:10.1175/1520-0450(1981)020<0802:AFLBLM>2.0.CO;2, 1981. 8443

Sheng, J.-X., Weisenstein, D. K., Luo, B.-P., Rozanov, E., Stenke, A., Anet, J., Bingemer, H., and Peter, T.: Global atmospheric sulfur budget under volcanically quiescent conditions: aerosol-chemistry-climate model predictions and validation, J. Geophys. Res.-Atmos., 120, 256–276, doi:10.1002/2014JD021985, 2015. 8441

SPARC: Assessment of Stratospheric Aerosol Properties, edited by: Thomason, L. and Peter. T., WCRP-124 WMO/TD-No. 1295, 4, 2006. 8441, 8446, 8451, 8453

Thomason, L. W., Poole, L. R., and Deshler, T.: A global climatology of stratospheric aerosol surface area density deduced from Stratospheric Aerosol and Gas Experiment II measurements: 1984–1994, J. Geophys. Res.-Atmos., 102, 8967–8976, doi:10.1029/96JD02962, doi:10.1029/96JD02962, 1997. 8441

Tjemkes, S., Patterson, T., Rizzi, R., Shephard, M., Clough, S., Matricardi, M., Haigh, J., Höpfner, M., Payan, S., Trotsenko, A., Scott, N., Rayer, P., Taylor, J., Clerbaux, C., Strow, L., DeSouza-Machado, S., Tobin, D., and Knuteson, R.: The {ISSWG} line-by-line inter-comparison experiment, J. Quant. Spectrosc. Ra., 77, 433–453, doi:10.1016/S0022-4073(02)00174-7, 2003. 8444

AMTD
8, 8439–8481, 2015

Tournier, B., Blumstein, D., and Cayla, F. R.: IASI level 0 and 1 processing algorithms description, in: Proc. 12th International TOVS Working Group, Lorne, Australia, 2002. 8444

van de Hulst, H.: Light Scattering by Small Particles, Dover Books on Physics Series, Dover Publications, Mineola, New York, USA, available at: http://books.google.fr/books?id=PlHfPMVAFRcC (last access: 7 August 2015), 1957. 8445

von Glasow, R., Bobrowski, N., and Kern, C.: The effects of volcanic eruptions on atmospheric chemistry, Chem. Geol., 263, 131–142, doi:10.1016/j.chemgeo.2008.08.020, 2009. 8441

Yu, P., Toon, O. B., Neely, R. R., Martinsson, B. G., and Brenninkmeijer, C. A. M.: Composition and physical properties of the Asian Tropopause Aerosol Layer and the North American Tropospheric Aerosol Layer, Geophys. Res. Lett., 42, 2540–2546, doi:10.1002/2015GL063181, 2015GL063181, 2015. 8441

AMTD
8, 8439–8481, 2015

Table 1. Total number concentrations and effective number concentrations used in the present work.

Number concentration [particles cm^{-3}]	Effective number concentration [particles cm^{-3}]
8	2.52
9	2.83
10	3.15
12	3.78
15	4.72
20	6.83
25	7.87
30	9.45

AMTD
8, 8439–8481, 2015

Table 2. Mean radii and effective radii used in the present work.

Mean radius [μm]	Effective radius [μm]
0.06	0.16
0.07	0.18
0.08	0.21
0.10	0.26
0.15	0.39
0.20	0.52
0.30	0.79
0.40	1.05

AMTD
8, 8439–8481, 2015

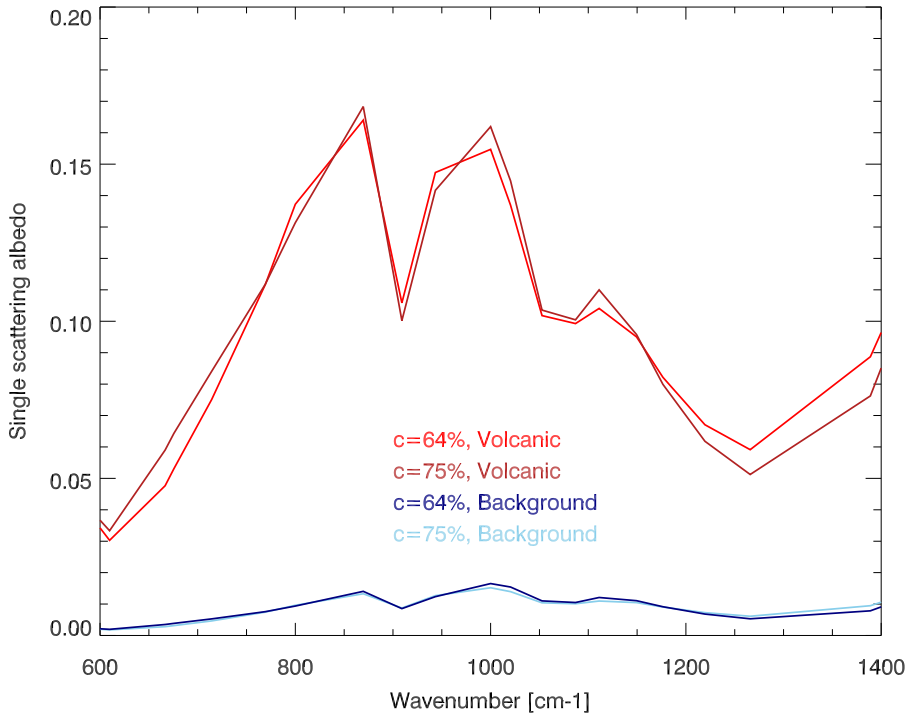

Figure 1. Spectral single scattering albedo, in the spectral range 600–1400 cm^{-1}, for sulphate aerosol layers with different H_2SO_4 mixing ratios (64 and 75 %, at 213–215 K), for typical background size distribution (dark and light blue lines) and for a moderate volcanically-perturbed size distribution (dark and light red lines). See the text for further details.

AMTD
8, 8439–8481, 2015

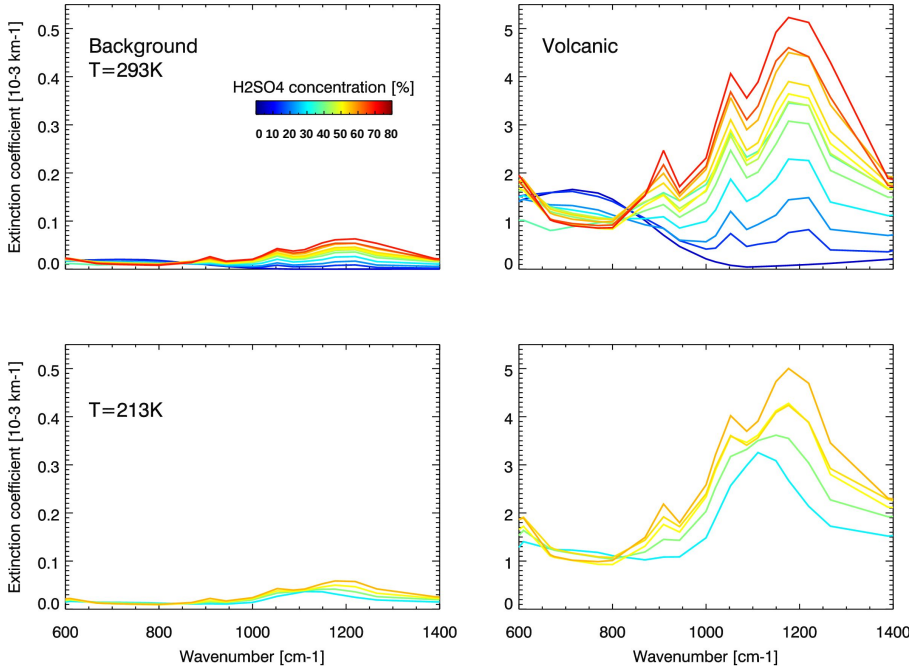

Figure 2. Spectral extinction coefficients for sulphate aerosol layers with different H_2SO_4 mixing ratios, from 0 to 80 % as indicated by the colorbar, and temperatures of 293 K (upper row) and 213 K (bottom row). Different mixing ratiotemperature combinations are shown, depending on the availability in the refractive indices dataset of Biermann et al. (2000). The extinction coefficients are shown for a typical background size distribution (left column) and for a moderate volcanically-perturbed size distribution (right column). See the text for further details.

AMTD
8, 8439–8481, 2015

Sensitivity of TIR satellite instruments to UTLS sulfate aerosols

P. Sellitto and B. Legras

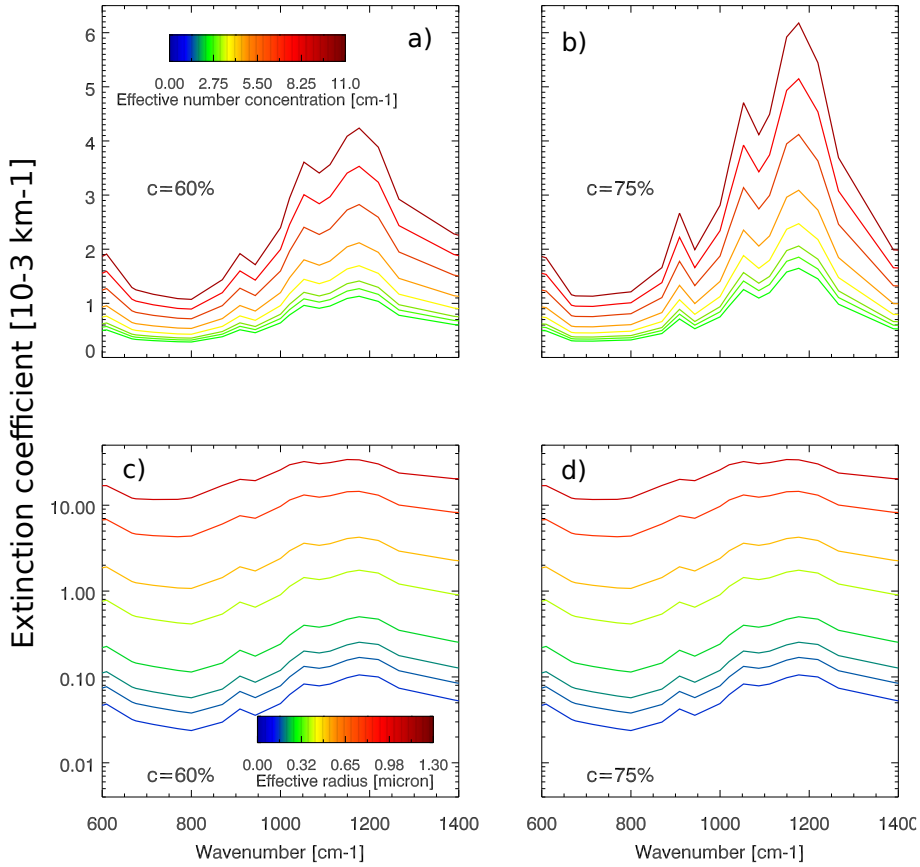

Figure 3. Spectral extinction coefficient for a sulphate aerosol layer, as a function of: **(a, b)** the effective number concentration N_e (different number concentrations in different colors, see colorbar), **(c, d)** the effective radius r_e (different radii in different colors, see colorbar). Sulphate aerosols layers with 60 and 75 % (values indicated in the plots) H_2SO_4 mixing ratios, at 213–215 K are considered. Please note the logarithmic ordinate in **(c, d)**.

AMTD
8, 8439–8481, 2015

Sensitivity of TIR satellite instruments to UTLS sulfate aerosols

P. Sellitto and B. Legras

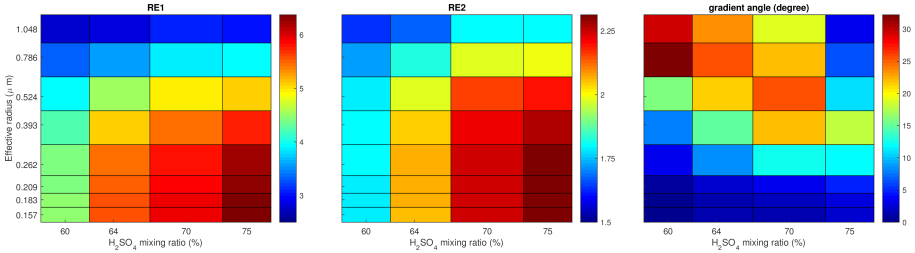

Figure 4. RE1 **(a)** and RE2 **(b)** as a function of the effective radius and H_2SO_4 mixing ratio. Please note the different scaling of the colorbars. Arcosine of the scalar product $\nabla RE1 \cdot \nabla RE2$ **(c)**. The gradients are normalized.

AMTD
8, 8439–8481, 2015

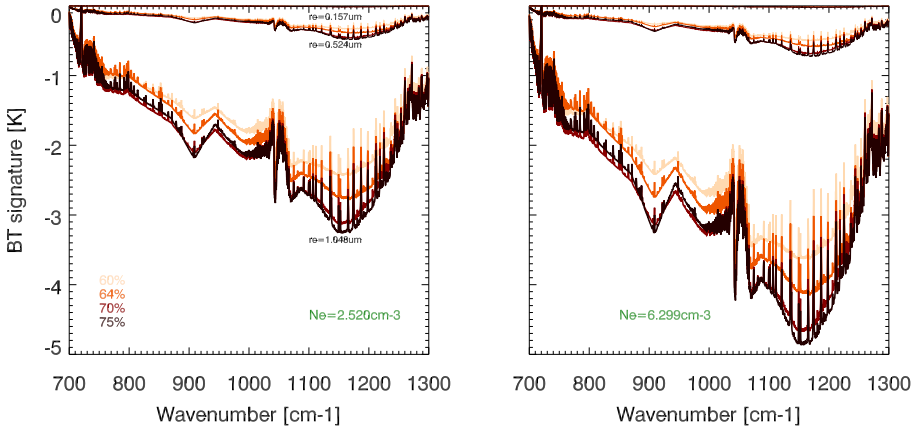

Figure 5. BT signature of sulphate aerosol layers, for effective number concentrations of 2.52 (left panel) and 6.30 particles cm^{-3} (right panel), for effective radii of 0.16, 0.52 and 1.05 µm (see text in the figures) and H_2SO_4 mixing ratio of 60, 64, 70, 75 % (in different colors).

AMTD
8, 8439–8481, 2015

Sensitivity of TIR satellite instruments to UTLS sulfate aerosols

P. Sellitto and B. Legras

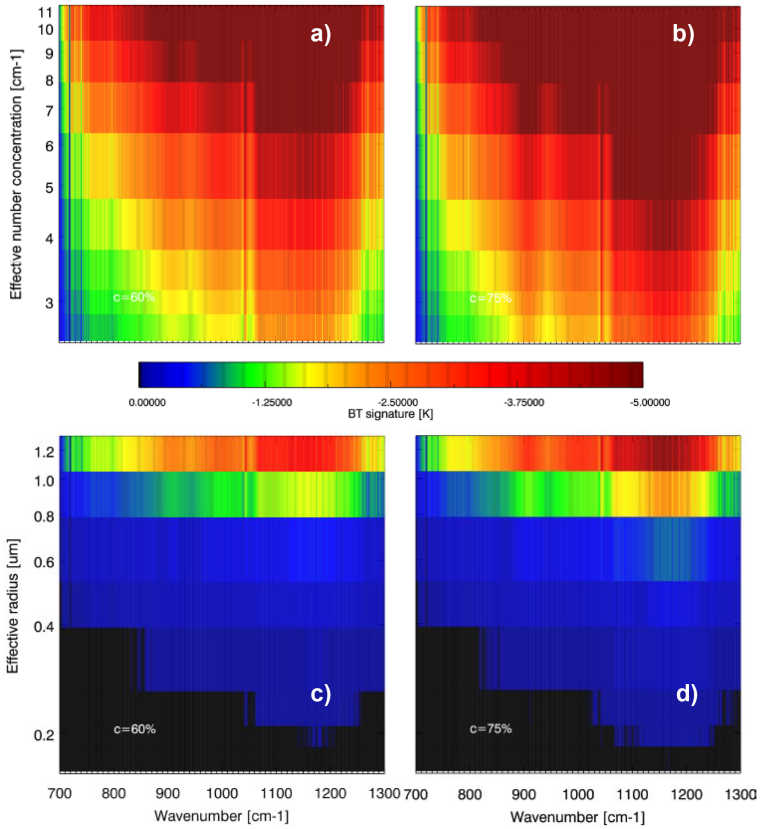

Figure 6. Spectral BT signatures for a sulphate aerosol layer at about 150 hPa altitude, as a function of the effective number concentration N_e for a fixed effective radius $r_e = 0.79\,\mu m$ **(a, b)**, and as a function of the effective radius r_e for a fixed effective number concentration $N_e = 7.87$ particles cm^{-3} **(c, d)**. Sulphate aerosols layers with 60 % **(a, c)** and 75 % **(b, d)** H_2SO_4 mixing ratios, at 213–215 K, are considered.

AMTD
8, 8439–8481, 2015

Sensitivity of TIR satellite instruments to UTLS sulfate aerosols

P. Sellitto and B. Legras

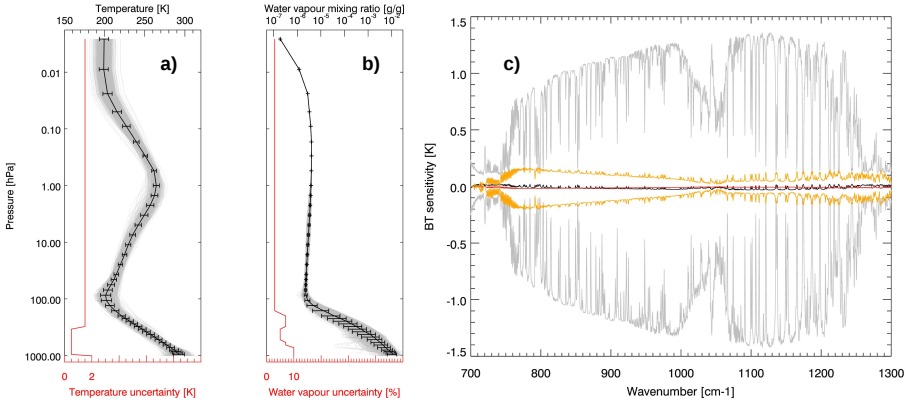

Figure 7. Individual (grey) and average TIGR tropical vertical profiles with standard deviations (black), for temperature **(a)** and water vapour mixing ratio **(b)**. The standard deviation of the gaussian noise used to generate the perturbed profiles is in red in both figures; spectral BT sensitivity for temperature profile (mean differences in black, one-standard deviation interval in grey) and water vapour profile variability (mean differences in red, one-standard deviation interval in orange) **(c)**. See text for further details on how this sensitivity is evaluated.

AMTD
8, 8439–8481, 2015

Sensitivity of TIR satellite instruments to UTLS sulfate aerosols

P. Sellitto and B. Legras

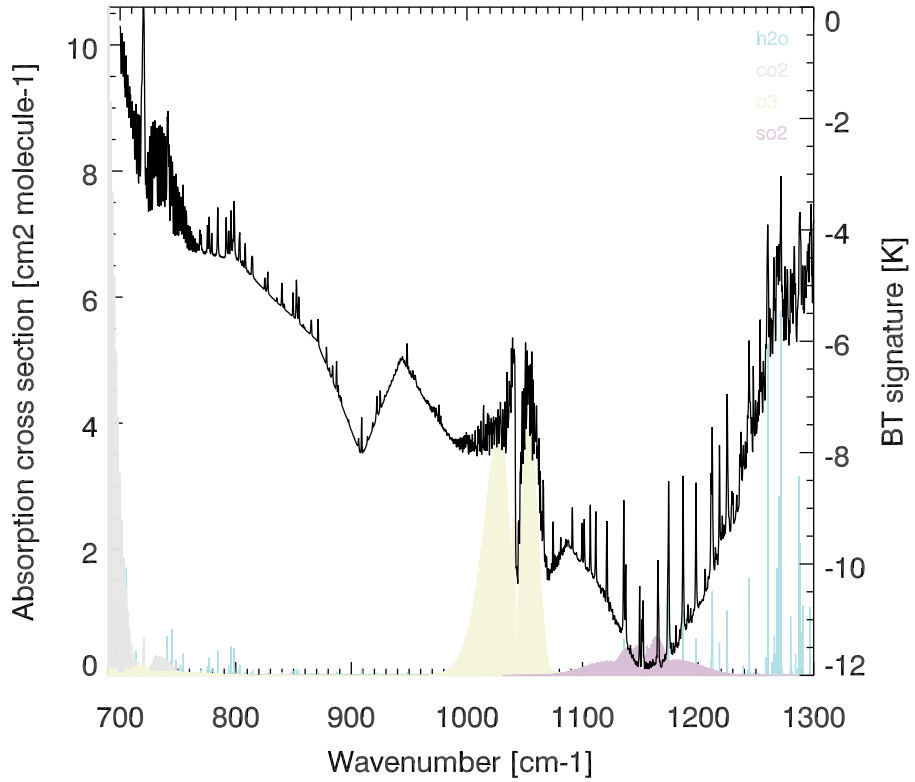

Figure 8. Absorption cross sections of water vapour (multiplied by a factor 30 to enhance visualization, sky blue), carbon dioxide (grey), ozone (yellow) and sulphur dioxide (violet) in the spectral range 700–1300 cm^{-1}. A typical sulphate aerosol BT signature is overplot (black).

AMTD
8, 8439–8481, 2015

Sensitivity of TIR satellite instruments to UTLS sulfate aerosols

P. Sellitto and B. Legras

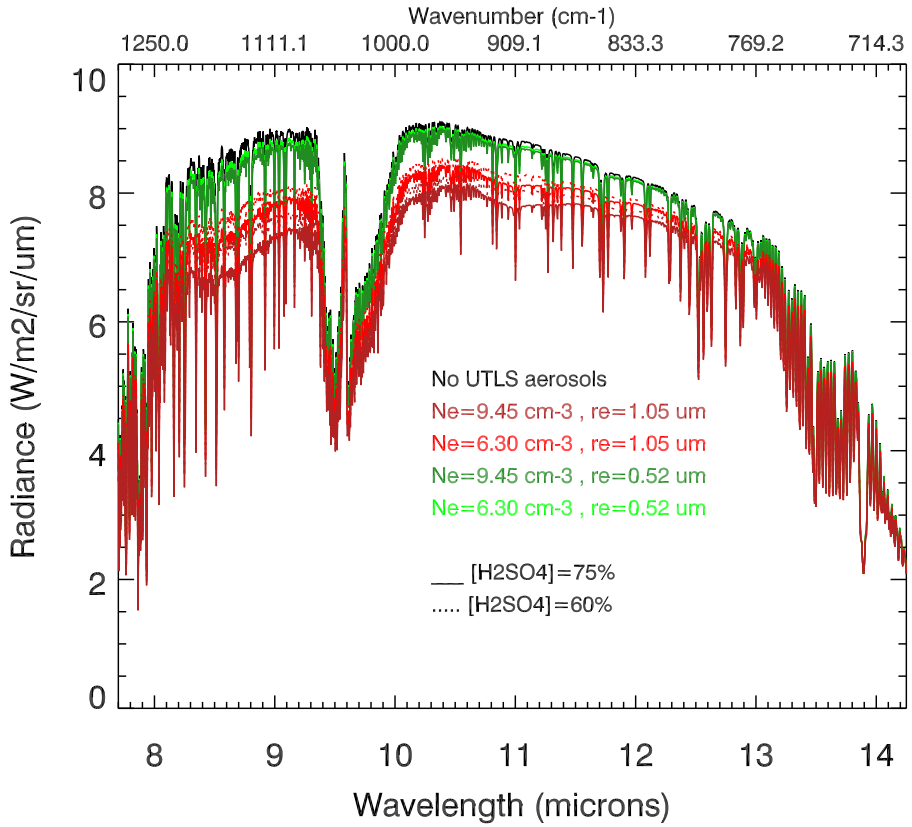

Figure 9. Simulated radiances for baseline no UTLS aerosol conditions (black) and different UTLS aerosols with different H_2SO_4 mixing ratios, effective radii and effective number concentrations (light and dark green and red, please see legend for details). The ascissa is expressed in both wavelength (to more readily compare with Fig. 1 of Corradini et al., 2009) and wavenumber.

AMTD
8, 8439–8481, 2015